

Contracting Skeletal Kinematic Embeddings for Anomaly Detection

Alessandro Flaborea^{a,*}, Guido Maria D’Amely di Melendugno^a, Stefano D’Arrigo^b, Marco Aurelio Sterpa^b, Alessio Sampieri^b, Fabio Galasso^a

^a*Department of Computer Science, Sapienza University of Rome, Italy*

^b*Department of Computer, Control and Management Engineering, Sapienza University of Rome, Italy*

Abstract

Detecting the anomaly of human behavior is paramount to timely recognizing endangering situations, such as street fights or elderly falls. However, anomaly detection is complex, since anomalous events are rare and because it is an open set recognition task, i.e., what is anomalous at inference has not been observed at training. We propose COSKAD, a novel model which encodes skeletal human motion by an efficient graph convolutional network and learns to COntract SKeletal kinematic embeddings onto a latent hypersphere of minimum volume for Anomaly Detection. We propose and analyze three latent space designs for COSKAD: the commonly-adopted Euclidean, and the new spherical-radial and hyperbolic volumes. All three variants outperform the state-of-the-art, including video-based techniques, on the *ShangaiTechCampus*, the *Avenue*, and on the most recent *UBnormal* dataset, for which we contribute novel skeleton annotations and the selection of human-related videos. The source code and dataset will be released upon acceptance.

Keywords: anomaly detection, open-set recognition, hyperbolic geometry, kinematic skeleton, graph convolutional networks

*Corresponding author

Email address: flaborea@di.uniroma1.it (Alessandro Flaborea)

1. Introduction

Anomaly Detection (AD) is a broad and well-studied field in computer vision, which aims to detect events that deviate from normality automatically [1]. More precisely, the task is to detect anomalous events in footage and label the corresponding frames as abnormal. AD is a complex and multifaceted field with applications beyond just video surveillance [2, 3]. Many techniques have been successfully applied in several real-world scenarios, including monitoring elderly individuals [4], industrial systems [5] and social networks [6].

While significant progress has been made in AD in recent years, this task still presents several challenges: (1) anomalous events are rare in real-world scenarios, and this reflects in the imbalanced distribution of normal and anomalous events in public AD datasets. (2) Anomalous events are challenging to identify since abnormal actions can involve either frenetic movements (e.g., fights) or very still postures (e.g., faints), resulting in a context-dependent definition of anomaly, which varies among public datasets. Furthermore, the same anomalous action can vary significantly among individuals, adding to the intra-class variation that must be considered. Finally, (3) when working with videos of humans, it is crucial to consider privacy and fairness concerns, such as avoiding violations of individuals’ rights or exploiting social biases.

In this work, we propose COSKAD. This novel end-to-end model infers abnormality COnttracting SKeletal (COSKAD) embeddings in the latent space and opens up a novel investigation of the latent metric space encoding the regular motions. The proposed method tackles all the limitations mentioned above. First, it adheres to the *One-Class-Classification* (OCC) [7, 8, 9, 10, 11, 12] protocol, which simulates the scarcity of abnormal events exposed in (1). Moreover, COSKAD exploits the compact spatiotemporal skeletal representation (cf. Fig. 1) of human motion instead of raw frames, typically employed with appearance-based methods. This modality comes with several advantages; first, recent work [13] in the motion-related fields of Pose Forecasting and Action Recognition has proven the superiority of this modality wrt the raw video frames for

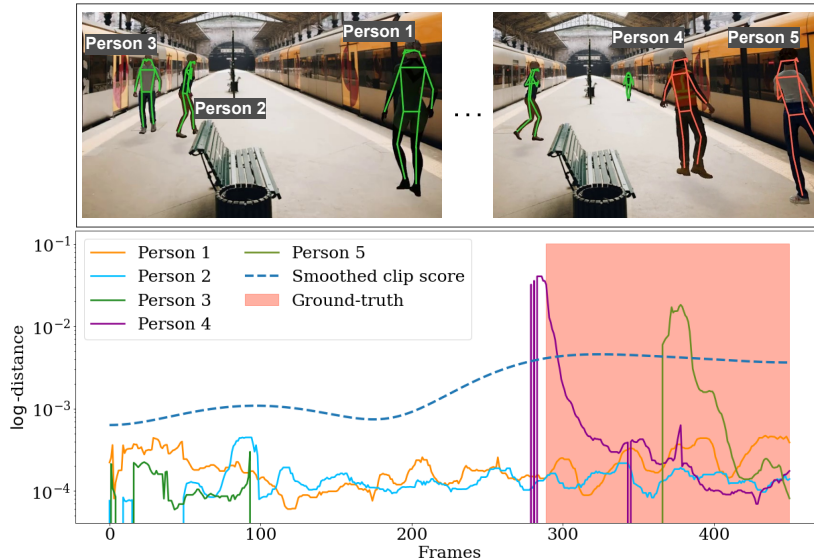


Figure 1: Anomaly score provided by COSKAD on a clip from the UBnormal dataset. COSKAD correctly classifies the motion of the two staggering characters (red skeletons in the upper-right picture) in the last part of the clip as anomalous.

motion representation. Exploiting this input modality, our proposed model is more robust to slight motion deformations that represent the intra-class variability described in (2) while preserving the ability to distinguish between different actions, e.g., walking vs. running, which is crucial in AD. Furthermore, modeling agents as kinematic graphs allows for separating the person detection task (handled as a preprocessing step) from the anomaly detection task, resulting in a more computationally efficient and context-agnostic method. Although skeletal representations are more compact than raw video frames, they contain the necessary information for effectively characterizing motions, as demonstrated by the state-of-the-art results of skeleton-based methods [9, 10, 11]. Finally, the skeletal representation is more privacy-preserving (3) since it ignores biometric details, representing all samples with anonymous tensors of coordinates. Consistently with this setting, we adopt the Human Related (HR)[10] split of the datasets, which corresponds to a version of the dataset that admits only

anomalies generated by humans, e.g., people fighting, disregarding anomalies coming from the context scene, e.g., a car proceeding on the pavement.

The proposed model comprises two founding components: an encoder and a projector module. Differently from previous related works, which use either ST-GCN [14, 15, 11], or a Recurrent Neural Network [10] to encode the human motion, COSKAD implements its encoder as a Space-Time-Separable Graph Convolutional Network [16]. As far as we know, this is the first study to adapt it for skeletal-based AD and to expose a comparison among different GCN-based encoders (presented in Sec. 5.1). The projector module draws inspiration from SSL, where it has been shown to play a crucial role [17, 18], which we confirm here in detailed ablation studies (cf. Sec. 5.2). Finally, we define a data-driven metric objective in the latent space to minimize the distance between the skeletal embeddings and a center. We call the distance minimization *contraction*, as it forces normality to concentrate around an origin. Dealing with a metric objective, we further propose a novel investigation of how the latent distribution might be altered, condensed, or expanded using the peculiar metric properties of three distinct manifolds: the Euclidean (\mathbb{R}^n), the Hyperbolic Space (\mathbb{H}^n), and the n-Sphere (\mathbb{S}^n). As far as we know, this is the first work to have studied different latent spaces for skeleton-based anomaly detection.

The proposed model is simple, lightweight, and effective, as we illustrate in extensive experiments, where COSKAD outperforms state-of-the-art (SoA) models (including some video-based techniques) on three challenging benchmarks: *HR-ShanghaiTechCampus* [15, 11], *HR-Avenue* [19, 10], and the recent *UBnormal* [20].

Additionally, we offer an ablative examination of several of our model’s key features. Beyond a thorough ablation study on the main modules of our proposed COSKAD, we also compare the encoder-based architecture proposed with an autoencoder and compare two alternative strategies to define the hypersphere center, extending the seminal study of [21].

Finally, we propose a novel HR version of UBnormal [20], dubbed *HR-UBnormal* as an additional contribution. We create HR-UBnormal by filter-

ing out its events to maintain human-related events only retain videos that are anomalous because of human actions, not due to the scene itself, e.g. we remove scenes of fire and car accidents unless people are involved. We leverage an established Pose Estimator [22] and refine its results with a Pose Tracker [23], to extract the human poses in each UBnormal’s video frame. So HR-UBnormal contains human-related anomalies and the human skeletons at all frames, inspected for accuracy and temporal consistency.

To summarize, the contribution of this paper is threefold:

- We introduce COSKAD, a simple, end-to-end, and effective model that surpasses SoA results on three public benchmarks.
- We conduct an in-depth study on three different manifolds as latent spaces, and explore their intrinsic properties, and thoroughly analyse their effects on our novel AD system.
- We introduce a new *HR* version of UBnormal with a filtered selection of clips featuring human-related events and an extended set of human body pose annotations.

2. Related work

Anomaly Detection (AD) is a multi-faceted field with applications in several domains (see [24, 25, 26] for surveys). This work focuses on Skeleton-based anomaly detection, a type of video-based AD that involves analyzing the movements and poses of human bodies in a video. In this section, we compare works that most closely relate to ours, distinguishing error-based and score-based video AD techniques and skeleton-based models.

2.1. Video AD

Early proposed methods analyze the trajectories of agents in the video to unearth those that differ from normality [27, 28, 29]. More recent deep learning

methods for Video AD can be roughly collected into two categories: error-based or score-based.

Error-based methods. These methods attempt to detect anomalies through a generative process in which a model produces new video frames, which are then compared with ground truth. These methods assume that a model trained with only normal data will struggle to generate the anomalous frames, producing a more significant error that can be directly used as the anomaly score. [7] used convolutional AutoEncoder (AE) and defined the input volume as a stack of sequential grayscale frames. [30] during the training phase builds a memory of the most representative normal poses. During the inference phase, for each sample, it finds the most similar example in memory and estimates its ground truth distance. Unlike these methods, COSKAD relies on a GCN-encoder, an ideal tool for exploring relationships between body joints over time in the kinematic graph and extracting semantically consistent latent embeddings.

Score-based methods. These approaches have been extensively studied [31, 32, 21, 33]. They derive abnormality in videos by monitoring some quantity extracted from the embeddings produced by the deep network. For example, [34] proposed a two-stage method in which videos are divided into cubic patches and first analyzed with Gaussian classifiers to exclude the least relevant patches, e.g., background. Then the remaining candidates are processed by a more complex CNN. In contrast, COSKAD looks at the latent space positions occupied by input embeddings to derive clues of abnormality. While working with images rather than video, Deep Support Vector Data Description (DSVDD) [21] and OC4Seq [33] are two methods related to COSKAD, as both employ a DSVDD objective seeking to minimize a sphere enclosing the generated embeddings. While we also employ an SVDD objective, our model learns in an end-to-end way to map the representation of the normal samples in the latent space while encoding semantic representations thanks to its separable GCN encoder. As far as we know, this work is the first to propose the SVDD objective for Video AD with skeleton-based representations.

2.2. Skeleton-based AD

[10] first introduces the skeleton-based representation in AD; their method presents a two-branches architecture for reconstruction and forecasting modeled as GRUs. [9] sets up the problem as motion forecasting and defines their model by stacking layers of ST-GCN [14] followed by an MLP forecasting module. While they introduce the use of GCN, the adjacency matrix is fixed and does not allow the exploration of intra-frame and intra-joint relationships, improving spatio-temporal features encoding [16]. [11] proposes a two-stage network in which they train an autoencoder (built on ST-GCN [14]), and, in the second stage, it clusters the produced embeddings in the latent space. These clusters should represent the normality styles present in the train set, but it is challenging to spot the optimal number of clusters. Differently, COSKAD has an end-to-end approach and solves the problem of the number of clusters by forcing the entire train set into the same latent region, constraining the distances to a common center.

3. Methodology

In this section we describe our proposed model focusing on its modules and the steps taken to train and assess it.

We assume the human body kinematics to be available as skeleton representations for a few given frames (cf. Sec. 4.1.1 for the details on the skeleton sequence extractions for the proposed HR-UBnormal dataset). These spatio-temporal graphs input are fed to COSKAD which, as illustrated in Fig. 2, relies on two key components: a separable graphs encoder and a projection module. The encoder processes the input graph and produces embeddings representing the motion of each individual. The projector adapts the embedding provided by the encoder for the mapping in the latent space. Both modules are jointly trained with a spatial minimization objective, which aims to catch the correspondences among samples belonging to the same class. Finally, we define a novel metrical objective in the latent space in order to guide the training, and

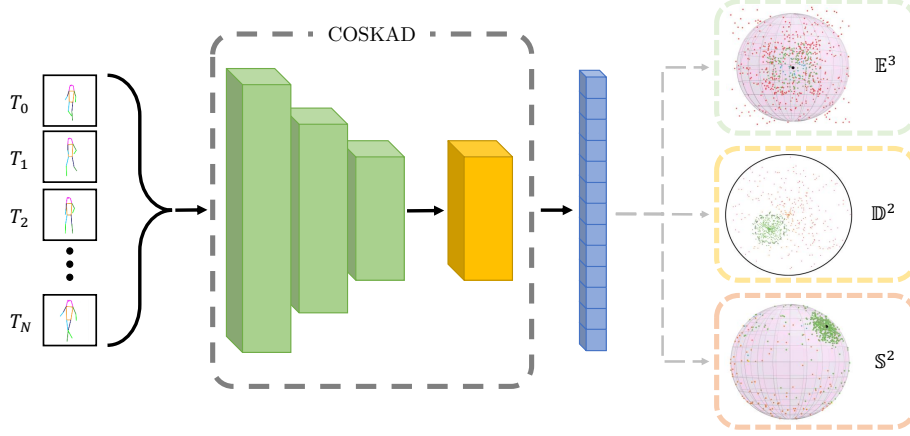


Figure 2: The overall architecture of COSKAD. The model combines a projector module (yellow block in the figure) with a GCN-based encoder (green blocks). After projection, the latent representation (blue vector in the figure) is embedded into the latent space, which forces them to accumulate in a narrow region of the latent space, so the sequences mapped further away from the center are interpreted as anomalous during inference. We propose and evaluate 3 variants of the latent space: *Euclidean* \mathbb{R}^n , *spherical* \mathbb{S}^n , and the *Hyperbolic* modeled with the Poincaré Disk \mathbb{D}^n .

consider three different manifolds as latent spaces: the *Euclidean Space* (\mathbb{E}^n), the *Poincaré Disk* (\mathbb{D}^n), and the *n-Sphere* (\mathbb{S}^n), to inherit their specific metric properties.

Formulation. The motion trajectories consist of V joints per actor in each frame tracked across all the frames (T_{actor}) where the actor is present. We apply a temporal sliding windows crop on the trajectories to get sequences of V joints’ spatial positions for T adjacent time frames. Finally, we organize the input signal as a graph $\mathcal{G} = (\mathcal{V}, \mathcal{E})$, with TV nodes $x_i \in \mathbb{R}^C$, where $C = 2$ stands for the x, y joint coordinates, and with edges $(i, j) \in \mathcal{E}$, represented by a spatio-temporal adjacency matrix $A^{st} \in \mathbb{R}^{VT \times VT}$, relating all joints to all others across all observed time frames.

3.1. Encoder & Projection module

We encode the body kinematics of a person with a SoA variant[16] of Graph Convolutional Network (GCN) [35]. GCNs are the go-to choice in the kinematic-

related fields of Pose Forecasting [16, 36, 13] and action recognition [14, 37]. COSKAD leverages a separable GCN-encoder designed to capture spatio-temporal signals and produce consistent features. Specifically, the encoding performs a factorization of the adjacency matrix A into two learnable submatrices (A_s, A_t) responsible for spatial and temporal interconnections, respectively. $A_s \in \mathbb{R}^{T \times V \times V}$, the *spatial adjacency matrix*, learns the relationships between different joints in each frame by learning their interdependence. In contrast, $A_t \in \mathbb{R}^{V \times T \times T}$, the *temporal adjacency matrix* deals with the connections between different temporal instants for each joint.

This strategy, also adopted by [16] in the context of pose forecasting, ensures effective encoding of the spatio-temporal features of the input graph by learning and exploiting the joint-joint and time-time relationships that characterize human motion. In addition, this factorization results in a considerable reduction in the number of parameters ($\sim 4x$ with respect to a plain GCN) since it does not consider the relationships between different joints in different frames.

We formulate a single encoder layer as:

$$X^{l+1} = \sigma(A_s A_t X^l W) \quad (1)$$

where X^l is the input from the previous layer, $W \in \mathbb{R}^{C \times C'}$ are learnable weights and σ an activation function. We stack four separable GCN layers interleaved with residual connections to encode the entire input sequence. Overall, the results of our ablation studies (cf. Sec. 5.1) suggest that the separable GCN is the best encoder among the GCN architectures we evaluated.

Reminiscent of recent works in Self-Supervised Learning (SSL) [18, 17], we explicitly define a projector module to refine the Encoder representation and accommodate it in the latent space. The projector comprises two identical blocks that iteratively process their input with a Fully Connected Module followed by a ReLU non-linearity and a Batch Normalization [38] layer. Despite its simplicity, we found it beneficial to add this module, as shown in Sec. 5.2.

3.2. Objective

The OCC formulation requires that the train sets contain elements of a single class. Therefore, the design of the objective function is crucial, as it can only exploit the similarities that normal samples exhibit. Many existing methods [30, 39, 10, 8, 9, 40] formulate the anomaly score using a proxy task, such as the reconstruction error. In Sec. 5.4, we experimentally confirm that this is suboptimal, as maintained in [41] since it does not align directly with the inference AD objective.

In this work, we define a metric objective that encourages the model to arrange the train samples in a narrow region in the latent space: inspired by [21], the objective is defined as:

$$\min_{\mathcal{W}} \frac{1}{N} \sum_{i=1}^N d(\Phi(x_i, \mathcal{W}), c) + \alpha f(\mathcal{W}) \quad (2)$$

Where Φ represents the mapping in the latent space defined by COSKAD, \mathcal{W} being the set of its parameters, $x_i \in \mathbb{R}^{T \times V \times C}$ is an input sample, d is a metric defined in the latent space, f is a weight decay regularizing function, and c is the center of the hypersphere. We follow [21] and initialize c by taking the average of the final embeddings after an initial forward pass. Then, [21] suggests training the model with the parameter c fixed. We argue that this practice may harm the training, leading to a non-optimal solution since the center is precalculated and its position does not evolve with the learning.

Differently from [21], we introduce a novel and more tailored data-driven dynamic for the center: at the beginning of each training epoch, the position of the center is refined to be the centroid of the data’s projection in the latent space. The benefit of this moving center is twofold. First, a data-driven center relieves the encoder and the projector learning not being constrained to accumulate projection around a fixed point. Secondly, it encourages COSKAD to explore the latent space to find a region that accommodates the representations, which we show to be beneficial in Sec. 5.3, especially when the hyperbolic manifold is set to be the latent space.

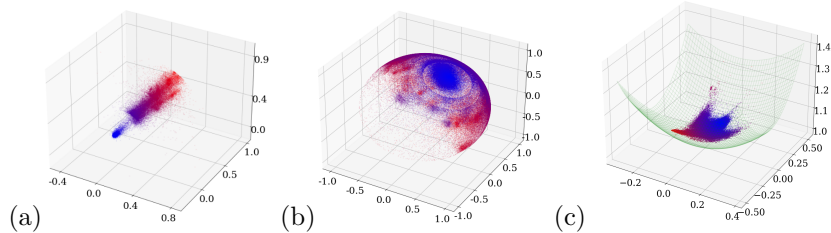


Figure 3: Visualization of the UBnormal test set’s latent vectors embedded in three different manifold: (a) Euclidean, (b) spherical and (c) hyperbolic. We retain the three dimensions with the highest variance and color-code the points according to their distance from the center, from blue (closest) to red (furthest). Distance is intended as the L^2 norm in the Euclidean case, the *cosine distance* on \mathbb{S}^n , and the *Poincaré distance* for the hyperbolic embeddings. In the hyperbolic case, we highlight in green the hyperboloid onto which the embeddings are projected for better visualization.

3.3. Latent Spaces

We propose to consider three diverse manifolds for embedding the input sequences. In fact, the objective of Eq. 2 forces the model to focus on features corresponding to common characters in the embeddings extracted from the encoder and to reduce their distances from a center iteratively. As a result, the method relies on a metric which, in turn, depends on the metric space \mathcal{L} chosen as the latent space. Motivated by this, we are the first to define the same objective on three manifolds, each with its own specific metric: the *Euclidean space* \mathbb{R}^n , the *spherical space* $\mathbb{S}^n \subset \mathbb{R}^{n+1}$, and the *Hyperbolic space* $\mathbb{H}^n \subset \mathbb{R}^{n+1}$. These spaces have a different curvature that causes the distance to behave differently in each manifold.

3.3.1. Euclidean Latent Space

When $\mathcal{L} = \mathbb{R}^n$, the distance coincides with the L^2 metric $d_E(x, y) = \|x - y\|_2$, and the model is defined substituting the distance d with d_E in Eq. 2.

3.3.2. n -Sphere Latent Space

With $\mathcal{L} = \mathbb{S}^n$, we modify the proposed COSKAD model, building on top of the *S-VAE* presented in [42]. We dub the model *COSKAD-radial* since it

constrains inputs onto the spherical surface with a fixed radius $\mathbb{S}^n = \{x \in \mathbb{R}^{n+1} : \|x\|_2 = 1\}$; the posterior of the normal data approximates a Power Spherical distribution $q_X(x; \mu, \kappa)$ [43], with a constraint $L_{dir} = \frac{1}{N} \sum_{i=1}^N (1 - x \cdot c)$ to push the samples close to the empirical mean direction c . The target loss is $L = \gamma L_{rec} + \phi L_{dir} + \beta L_{KL}$, where L_{rec} defines the objective for the Variational AutoEncoder reconstruction, L_{KL} is the Kullback-Leibler divergence, $\gamma, \phi, \beta \in \mathbb{R}$ hyperparameters. The anomaly score is solely given by the *cosine distance* between any sample x on \mathbb{S}^n and the empirical mean c computed at train time.

3.3.3. Hyperbolic Latent Space

When $\mathcal{L} = \mathbb{H}^n$, we model it with the *Poincaré Ball* which coincides with the unit euclidean open ball \mathbb{D}^n endowed with the distance

$$d_{\mathbb{H}}(x, y) = \text{arcosh} \left(1 + \frac{2\|x - y\|^2}{(1 - \|x\|^2)(1 - \|y\|^2)} \right). \quad (3)$$

The distances between the points on this manifold increase exponentially with distance from the origin O . To take full advantage of this property, we let the cluster center move in the Poincaré Ball in a data-driven fashion, but we also experienced defining the center as a fixed point, as detailed in Sec. 5.3. In Fig. 3, comparing the Euclidean (a) with the Hyperbolic (c) case, the effect of this distance is shown: in the Euclidean case, farther points tend to be more spread since the hyperbolic distance $d_{\mathbb{H}}$ ensures a stronger attraction towards the center, i.e. $d_{\mathbb{H}}$ grows exponentially with the distance from the center. In this case, the model is obtained from COSKAD by adding a projection layer $\exp_0 : \mathbb{R}^{n+1} \rightarrow \mathbb{D}^n$, which performs the exponential mapping to get the hyperbolic representation in \mathbb{D}^n . Thus, the objective defined in Eq. 2 becomes:

$$\min_{\mathcal{W}} \frac{1}{N} \sum_{i=1}^N d_{\mathbb{H}}(\exp_0(\Phi(x_i, \mathcal{W})), c) + \alpha f(\mathcal{W}). \quad (4)$$

3.4. Anomaly Score

At inference time, the anomaly score s for each sample x (representing a single agent in a time window composed by T frames $\{f_1, f_2, \dots, f_T\}$) is defined

as the distance of its COSKAD embedding from the center c :

$$s(x) = d(\Phi(x, \mathcal{W}), c). \quad (5)$$

To score a single frame \bar{f} , for each agent p , we first collect all the windows involving p in a set w^p , and we restrict this set picking only the windows containing \bar{f} to a set $w_{\bar{f}}^p$. Then, we calculate the score through Eq. 5 and thus set the score for p at frame \bar{f} to be the mean of those scores:

$$s^p(\bar{f}) = \frac{1}{|w_{\bar{f}}^p|} \sum_{x \in w_{\bar{f}}^p} s(x). \quad (6)$$

Finally, we get the score for a single frame \bar{f} by a max pooling operation over all the agents present in the scene at frame \bar{f} :

$$s(\bar{f}) = \max_{p \in P_{\bar{f}}} \{s^p(\bar{f})\}, \quad (7)$$

where $P_{\bar{f}}$ is the collection of all the people present in the clip at frame \bar{f} .

4. Experiments

In this section, we assess the performance of COSKAD on three public benchmarks against the state-of-the-art methods. The section first illustrates the experimental setup, then discusses the results on the recent *UBnormal* dataset, on its proposed HR version, and on the established benchmarks of *HR-Avenue* and *HR-STC*.

4.1. Benchmarks and Evaluation

We benchmark our novel COSKAD on four challenging datasets. The following sections describe the datasets we employed, along with a discussion of the current state-of-the-art and how COSKAD compares to it. First, we discuss the experiments on the recent UBnormal [20] dataset and its proposed HR version. Then, we detail the experiments on the established benchmarks of *HR-Avenue* [19] and *HR-STC* [15]. Refer to Table1 for the primary dataset features.

Dataset	# frames					
	<i>Total</i>	<i>Training</i>	<i>Validation</i>	<i>Test</i>	<i>Normal</i>	<i>Abnormal</i>
Avenue [19]	43,499	28,175	-	15,324	25,891	17,608
STC [15]	317,398	274,515	-	42,883	300,308	17,090
UBnormal [20]	236,902	116,087	28,175	92,640	147,887	89,015
HR-Avenue [10]	42,883	28,175	-	14,708	25,891	16,992
HR-STC [10]	313,212	274,515	-	38,697	297,090	16,122
HR-UBnormal (<i>Proposed</i>)	234,751	116,087	28,175	90,489	147,887	86,864

Table 1: An overview of the three datasets chosen, CUHK Avenue, ShanghaiTech Campus, and UBnormal, as well as their human-related versions.

4.1.1. UBnormal

The UBnormal dataset is a recent and large dataset proposed for supervised anomaly detection. In contrast to other benchmarks, it is a synthetic dataset created with Cinema4D. Starting from 29 natural 2D images with different backgrounds (e.g., streets, train stations, office rooms), the authors obtain virtual 3D scenes. For each scene, they produced 19 clips, which encompass both normal and abnormal events. UBnormal adheres to the *Open Set* protocol so that the types of anomalous events in the training or validation split differ from those that populate the test set. UBnormal has several distinctive features. First, as illustrated in Table1, it contains more anomalous frames than those presented in CUHK Avenue or ShanghaiTechCampus. Additionally, UBnormal has labels for each anomaly at both the frame and pixel level, with annotations describing the anomalous actions (e.g., jumping, sleeping, stealing). The anomaly types in UBnormal are also more heterogeneous than Avenue or STC. Since COSKAD is trained in the OCC framework, we extract only the normal sample poses from the training set as input for the model during training. Conversely, we maintain the original validation and test split in this setting.

HR-UBnormal (Proposed). We propose HR-UBnormal as an extension of the original UBnormal dataset with kinematic motion representations and a

selected set of anomalies that relate only to human behaviors. AlphaPose [22] is first used to extract the poses, and PoseFlow [23] is used to track the skeletons throughout each video. We then filter out the non-human related anomalies. We remove the sub-sequences in which the only anomalous object was not a person (e.g., a car) or the anomaly cannot be detected using only body poses (e.g., fire in the scene). The list of deleted non-HR anomalous actions is present in the supplementary materials. As a result, we leave the validation set unaltered while eliminating the 2.32% of test set frames. Table 1 lists the total number of normal and abnormal frames.

Evaluation. We score each frame in a video as mentioned in Sec. 3.4. Then, we compare it with the ground-truth labels to set the *Area Under the Curve* (AUC) score, following the previous literature in Video AD [19, 20, 8, 10, 11, 44].

Comparison with SoA. We benchmark COSKAD against the state-of-the-art methods and we report the results in Tab. 2. The table includes comparisons of skeleton-based and appearance-based approaches, including supervised, weakly-supervised, and OCC techniques.

We include the following methods as competitors to our proposed COSKAD:

- (Sultani et al.)[3] extracts features from videos and splits them into positive and negative bags. The ranking loss between the instances of the two bags with the highest scores is then computed. Following [20], we include both the fine-tuned and the pre-trained version of the model.
- (Bertasius et al.)[45] applies self-attention separately on temporal and spatial video patches. Both this method and the previous one are appearance-based and supervised. We provide the results from [20], where [45] is assessed using three different sample rates.
- (Georgescu et al.)[44] is a weakly supervised, appearance-based method. It adopts an adversarial learning strategy in which pseudo-abnormal samples are employed in the learning process. In [20], they assessed the same model in a supervised setting by replacing the pseudo-anomalies with abnormal

		UBnormal		HR-UBnormal
		Validation	Test	Test
<i>S</i>	Sultani <i>et al.</i> [3] (pre-trained)	61.1	49.5	-
	Sultani <i>et al.</i> [3] (fine-tuned)	51.8	50.3	-
	Georgescu <i>et al.</i> [44] + UBnormal anom.	68.2	61.3	-
	Bertasius <i>et al.</i> [45] (1/4 sample rate. fine-tuned)	78.5	61.9	-
	Bertasius <i>et al.</i> [45] (1/8 sample rate. fine-tuned)	83.4	64.1	-
	Bertasius <i>et al.</i> [45] (1/32 sample rate. fine-tuned)	86.1	68.5	-
<i>WS</i>	Georgescu <i>et al.</i> [44]	58.5	59.3	-
<i>OCC</i>	Morais <i>et al.</i> [10] *	61.2	60.6	61.2
	Markovitz <i>et al.</i> [11] *	47.0	53.4	55.2
	Ours - <i>radial</i> *	71.6	62.9	63.4
	Ours - <i>euclidean</i> *	75.8	64.9	65.2
	Ours - <i>hyperbolic</i> *	76.4	65.0	65.5

Table 2: Results on the dataset UBnormal and its subset HR-UBnormal, measured in terms of AUC score. The blocks split the table according to the framework each method relies on, where *S*, *WS*, and *OCC* stand for *Supervised*, *Weakly-Supervised*, and *One-Class-Classification*, respectively. (*) indicates that the model is designed for skeleton-based anomaly detection. We highlight in bold our results, which should be directly compared to the other OCC methods.

sequences from UBnormal (in Tab. 2 we refer to this model as [44] + *UBnormal anom.*).

- (Markovitz et al.)[11] and (Morais et al.)[10] are OCC skeleton-based methods. The former performs a GCN encoding of sequences and then clusters the samples in the latent space. [10] uses a two branches RNN to reconstruct the pose of the input sequence and predict future frames. The reconstruction and prediction errors represent their measure of abnormality.

In Tab. 2, we assess our model on the recent UBnormal and the novel Human-Related version we propose. On both datasets, COSKAD outperforms all other OCC baselines comparable to ours. The table shows that for each of the three-volume shrinkage methods described in Sec. 3.3, COSKAD achieves SoA performance in both testing and validation splits. Our best performing model, COSKAD-*Hyperbolic* improves the performance of skeleton-based methods by

24,8% on the validation set, 7,2%, and 7% on UBnormal and HR-UBnormal test sets, respectively. Moreover, the proposed method outperforms [3] and the supervised version of [44] and is comparable with [45]. While the n-Sphere approach is still SoA, it looks to perform worse than the Euclidean and Hyperbolic methods in terms of results. This might be a consequence of the embeddings’ more dispersed distribution from the center, as visible in Fig.3.

4.1.2. CUHK Avenue & ShanghaiTech Campus

The **CUHK Avenue** dataset [19] contains 16 training videos and 21 testing videos with a total of 47 abnormal events recorded with different camera positions and angles. The HR-version [10] is obtained by removing frames where the (1) anomalous event is non-human, (2) the person involved is occluded, or (3) the main subject cannot be detected and tracked.

The **ShanghaiTech Campus** (STC) dataset [15] contains footage from 13 cameras around the campus with different light conditions and camera angles. It contains more than 300,000 total frames, and there is a total of 130 abnormal events, some of which are not present in other datasets (e.g., chasing, brawling). The HR-version [10] is obtained by removing 6 out of 107 test videos where the anomalous event is non-human.

Comparison with SoA. Tab. 3 shows our results for the two datasets containing only human-related anomalies. All of the baselines in the table are consistent with the OCC protocol; Conv-AE [7], and [8] are appearance-based methods, while all other methods are skeleton-based. On both *HR-STC* and *HR-Avenue*, COSKAD achieves SoA performance with the Euclidean version, reporting an AUC score of 77.1 and 87.8, respectively. Further, the Hyperbolic version of COSKAD achieves previous SoA performances (on par with [9]).

4.2. Experimental setup

Implementation details. We train our proposed COSKAD with Pytorch Lightning using two Nvidia P6000 GPUs for 80 epochs, with a learning rate of 0.0001 and ADAM [46] optimizer. The training time took 1.5 hours, which is

	Params.	HR STC	HR Avenue
Hasan <i>et al.</i> [7]	-	69.8	84.8
Liu <i>et al.</i> [8]	14M	72.7	86.2
Morais <i>et al.</i> [10]	25K	75.4	86.3
Markovitz <i>et al.</i> [11]	805K	74.8	58.1
Luo <i>et al.</i> [9]	8M	<u>76.5</u>	<u>87.3</u>
Ours - <i>radial</i>	285K	75.2	82.2
Ours - <i>euclidean</i>	240K	77.1	87.8
Ours - <i>hyperbolic</i>	240K	75.6	<u>87.3</u>

Table 3: Results on the HR-ShanghaiTech Campus and HR-Avenue, in terms of AUC score. The best results are formatted in boldface, second best is underlined.

a fraction of the training time of [11, 10]. We consider $V = 17$ key points to represent a pose and divide each agent’s motion history by adopting a sliding windows procedure (each window has a length of $T = 12$ frames with stride 1 so that windows overlap).

Pose normalization. Since the 2D positions of the joints refer to the frame, we normalize the poses to make them non-location dependent, following [10]. For all three datasets, we perform an additional normalization stage by applying RobustScaler to reduce the contribution of outliers, as also done in [10].

5. Ablation Studies

We report in this section additional results and experiments that have guided us in building COSKAD. This study focuses on ablating the proposed model’s two main components and compares two strategies concerning the center update and the scoring method. All the experiments presented in this section are performed on the UBnormal dataset and are conducted using the best-performer Euclidean and the Hyperbolic versions of COSKAD. Notably, each ablated model presented in this section achieves SoA performances.

Encoder			Projector			Center Update		Hyperbolic	UBnormal	
GCN[35]	ST-GCN[14]	Sep. GCN	Identity	Linear	Non-Linear	Static	Dynamic		Valid.	Test
✓					✓		✓		68.9	59.1
✓					✓		✓	✓	69.1	59.0
	✓				✓		✓		68.4	62.6
	✓				✓		✓	✓	72.3	60.3
		✓	✓			✓			72.7	64.5
		✓	✓			✓		✓	72.0	63.6
		✓	✓				✓		71.3	64.7
		✓	✓				✓	✓	72.9	64.5
		✓		✓		✓			69.8	64.2
		✓		✓			✓	✓	71.1	64.7
		✓			✓	✓			74.5	64.6
		✓			✓	✓		✓	74.0	63.1
		✓			✓		✓		75.8	64.9
		✓			✓		✓	✓	76.4	65.0

Table 4: Ablation on the components of the proposed method COSKAD. Red checkmarks indicate the technical choices we implement in the final model. The results are attained on the UBnormal dataset.

5.1. Encoder

As illustrated in Sec. 3.1, COSKAD is equipped with a separable GCN-Encoder to process the input graphs. The first to propose a GCN as a kinematic encoder in the context of anomaly detection was [9], while previous works rely on LSTM [47], such as [10]. For this reason, we compare our encoder with other established GCN architectures, such as a plain GCN [35] and the ST-GCN [14], which have been employed in [11, 9]. As reported in Tab. 4, the selected separable GCN attains the best results among competitors, showing an increase in performance of 9.8% and 10.2% over GCN[35] and 3.6% and 7.8% over ST-GCN[14] on the euclidean and hyperbolic models, respectively. This result confirms that separating the kinematic adjacency matrix in its spatial and temporal parts allows for improved input representations. Moreover, separating the adjacency matrix results in a significant reduction in parameters, yielding an encoder with only 31K parameters against 75K and 170K of {ST-GCN, GCN}-based encoders, respectively.

# Blocks	Euclidean		Hyperbolic	
	Validation	Test	Validation	Test
0	71.2	64.1	72.4	63.7
1	75.8	64.9	76.4	65.0
2	75.7	64.8	74.01	64.6

Table 5: Ablation on the depth of the Non-Linear projector proposed (cf. Sec.5.2).

5.2. Projector

The importance of the projector when dealing with representations and metric objectives has been studied thoroughly in the field of SSL [17, 18]. Following [17], we compare three different definitions for the projector: the *Identity* (No projector), *Linear* (two linear layers), and *Non-Linear* (one block of linear layer, non-linearity, and Batch Normalization [38] followed by another linear layer) projectors. In Tab. 4, we empirically confirm the results of [17], showing that a non-linear projector provides a boost in performance (+5.6%, +0.54% on validation and test, respectively) when compared to an Identity projector, i.e. directly using the output of the encoder. The Identity and Linear strategies provide similar results, showing that a non-linearity is needed to improve the representations in the latent space. As a further investigation, we also ablate the deepness of the non-linear projector module. Specifically, we assess our model against different versions of it with a naive non-linear decoder without any block, performing only Batch Normalization, a ReLU activation and a linear layer, and a deeper projector involving two non-linear blocks followed by a linear layer. As depicted in Tab. 5, a single non-linear block considerably increases performance, especially in the Hyperbolic setting (+2%). Since the COSKAD’s modules operate in euclidean spaces, we expect a similar result which exposes the greater need for a projector when dealing with non-euclidean latent spaces. Further, using more layers results in a slight degradation in performance when using either the Euclidean or the Hyperbolic latent space (−0.2%, −0.6%, respectively).

5.3. Center Update Strategy

Since the metric objective of our method seeks to minimize the distance between the latent representations and a point defined in the latent space, it is critical to choose the optimal rule to update the center position during training to achieve optimal mapping. [21] proposed to fix a point in the latent space and then perform training around it. We experiment with this method, dubbed *Static*, and compare it with a novel rule to update the center position, dubbed *Dynamic*, in Tab. 4. As can be seen, the *Dynamic* strategy provides the best result, especially in the hyperbolic space, with an increase of 3% wrt to its *Static* counterpart, while the gain in Euclidean space (+0.4%) is more marginal. We expected a similar behavior since the metric defined within the Poincaré Ball induces a distance that grows exponentially with the radius, therefore, when the learning center is left free to move, the model can take advantage of it. On the other hand, with the *Static* strategy, it can be challenging for the model to minimize the distances of the embeddings to the fixed center.

5.4. COSKAD AutoEncoder

We also consider a multi-task learning objective for COSKAD coupling the original objective illustrated in Eq. 2 with a reconstruction error; to do this, we included an additional module that acts as a decoder, allowing COSKAD to reconstruct the original poses. Altogether, this makes our proposed model a GCN AutoEncoder, dubbed COSKAD-AE, and the new module has been obtained by reversing the GCN-Encoder. Tab. 6 compares the performance of COSKAD-AE, trained with both reconstruction and hypersphere loss, against our best model. Three methods for calculating the anomaly score are possible: either the reconstruction or hypersphere loss can be employed alone (named s_{rec} and s_{hyp} , respectively in Tab. 6), or the two scores can be combined ($s_{rec} + s_{hyp}$). The best performances are achieved by the only hypersphere score. This is probably due to the Separable GCN-Encoder that, separately learning the trajectories of single joints and unified poses for each timeframe, exposes improved generalization that affects the s_{rec} providing better reconstructions.

Model	Training	Inference	UBnormal
COSKAD	L_{hyp}	s_{hyp}	64.9
		s_{rec}	63.0
COSKAD-AE	$L_{hyp} + L_{rec}$	s_{hyp}	64.1
		$s_{hyp} + s_{rec}$	63.4

Table 6: Performance evaluation of our proposed models with COSKAD-AE. AUC score is reported for the UBnormal dataset.

6. Conclusion

We have proposed a novel Skeleton-based anomaly detection method based on the minimization of latent vectors to a center, exploiting the properties of three different manifolds: Euclidean, hyperbolic, and spherical. We defined the minimization metrics and scoring and investigated the alterations in space induced by manifolds. By leveraging a principled GCN encoder and coupling it with a loss that matches the OCC objective, COSKAD outperforms SoA models on established benchmarks. On UBnormal, all three versions of the proposed COSKAD reach SoA performance, witnessing the representational power of our approach.

References

- [1] V. Chandola, A. Banerjee, V. Kumar, Anomaly detection: A survey, ACM computing surveys (CSUR) 41 (3) (2009) 1–58.
- [2] J. T. Zhou, J. Du, H. Zhu, X. Peng, Y. Liu, R. S. M. Goh, Anomalynet: An anomaly detection network for video surveillance, IEEE Transactions on Information Forensics and Security 14 (10) (2019) 2537–2550. doi: 10.1109/TIFS.2019.2900907.
- [3] W. Sultani, C. Chen, M. Shah, Real-world anomaly detection in surveillance videos, in: Proceedings of the IEEE conference on computer vision and pattern recognition, 2018, pp. 6479–6488.

- [4] B. Prenkaj, D. Aragona, A. Flaborea, F. Galasso, S. Gravina, L. Podo, E. Reda, P. Velardi, A self-supervised algorithm to detect signs of social isolation in the elderly from daily activity sequences, *Artificial Intelligence in Medicine* 135 (2023) 102454. doi:<https://doi.org/10.1016/j.artmed.2022.102454>.
URL <https://www.sciencedirect.com/science/article/pii/S09333365722002068>
- [5] D. J. Atha, M. R. Jahanshahi, Evaluation of deep learning approaches based on convolutional neural networks for corrosion detection, *Structural Health Monitoring* 17 (5) (2018) 1110–1128.
- [6] Y. Liu, S. Chawla, Social media anomaly detection: Challenges and solutions, in: *Proceedings of the 21th ACM SIGKDD International Conference on Knowledge Discovery and Data Mining*, 2015, pp. 2317–2318.
- [7] M. Hasan, J. Choi, J. Neumann, A. K. Roy-Chowdhury, L. S. Davis, Learning temporal regularity in video sequences, in: *Proceedings of the IEEE conference on computer vision and pattern recognition*, 2016, pp. 733–742.
- [8] W. Liu, W. Luo, D. Lian, S. Gao, Future frame prediction for anomaly detection—a new baseline, in: *Proceedings of the IEEE conference on computer vision and pattern recognition*, 2018, pp. 6536–6545.
- [9] W. Luo, W. Liu, S. Gao, Normal graph: Spatial temporal graph convolutional networks based prediction network for skeleton based video anomaly detection, *Neurocomputing* 444 (2021) 332–337.
- [10] R. Morais, V. Le, T. Tran, B. Saha, M. Mansour, S. Venkatesh, Learning regularity in skeleton trajectories for anomaly detection in videos, in: *Proceedings of the IEEE/CVF conference on computer vision and pattern recognition*, 2019, pp. 11996–12004.
- [11] A. Markovitz, G. Sharir, I. Friedman, L. Zelnik-Manor, S. Avidan, Graph embedded pose clustering for anomaly detection, in: *Proceedings of the*

- IEEE/CVF Conference on Computer Vision and Pattern Recognition, 2020, pp. 10539–10547.
- [12] M. Z. Zaheer, A. Mahmood, M. H. Khan, M. Segu, F. Yu, S.-I. Lee, Generative cooperative learning for unsupervised video anomaly detection (2022).
 - [13] S. Xu, Y.-X. Wang, L.-Y. Gui, Diverse human motion prediction guided by multi-level spatial-temporal anchors, in: European Conference on Computer Vision (ECCV), 2022, pp. 251–269.
 - [14] S. Yan, Y. Xiong, D. Lin, Spatial temporal graph convolutional networks for skeleton-based action recognition, Proceedings of the AAAI Conference on Artificial Intelligence 32 (Apr. 2018). doi:10.1609/aaai.v32i1.12328. URL <https://ojs.aaai.org/index.php/AAAI/article/view/12328>
 - [15] W. Luo, W. Liu, S. Gao, A revisit of sparse coding based anomaly detection in stacked rnn framework, in: Proceedings of the IEEE international conference on computer vision, 2017, pp. 341–349.
 - [16] T. Sofianos, A. Sampieri, L. Franco, F. Galasso, Space-time-separable graph convolutional network for pose forecasting, in: 2021 IEEE/CVF International Conference on Computer Vision (ICCV), 2021, pp. 11209–11218.
 - [17] T. Chen, S. Kornblith, M. Norouzi, G. Hinton, A simple framework for contrastive learning of visual representations (2020). doi:10.48550/ARXIV.2002.05709. URL <https://arxiv.org/abs/2002.05709>
 - [18] J. Grill, F. Strub, F. Altché, C. Tallec, P. H. Richemond, E. Buchatskaya, C. Doersch, B. Á. Pires, Z. D. Guo, M. G. Azar, B. Piot, K. Kavukcuoglu, R. Munos, M. Valko, Bootstrap your own latent: A new approach to self-supervised learning, CoRR abs/2006.07733 (2020). arXiv:2006.07733. URL <https://arxiv.org/abs/2006.07733>

- [19] C. Lu, J. Shi, J. Jia, Abnormal event detection at 150 fps in matlab, in: Proceedings of the IEEE international conference on computer vision, 2013, pp. 2720–2727.
- [20] A. Acsintoae, A. Florescu, M.-I. Georgescu, T. Mare, P. Sumedrea, R. T. Ionescu, F. S. Khan, M. Shah, Ubnormal: New benchmark for supervised open-set video anomaly detection, in: Proceedings of the IEEE/CVF Conference on Computer Vision and Pattern Recognition, 2022, pp. 20143–20153.
- [21] L. Ruff, R. Vandermeulen, N. Goernitz, L. Deecke, S. A. Siddiqui, A. Binder, E. Müller, M. Kloft, Deep one-class classification, in: International conference on machine learning, 2018, pp. 4393–4402.
- [22] H.-S. Fang, S. Xie, Y.-W. Tai, C. Lu, Rmpe: Regional multi-person pose estimation, in: ICCV, 2017, pp. 2334–2343.
- [23] Y. Xiu, J. Li, H. Wang, Y. Fang, C. Lu, Pose Flow: Efficient online pose tracking, in: BMVC, 2018.
- [24] D. Bogdoll, M. Nitsche, J. M. Zöllner, Anomaly detection in autonomous driving: A survey, in: Proceedings of the IEEE/CVF Conference on Computer Vision and Pattern Recognition, 2022, pp. 4488–4499.
- [25] W. Hilal, S. A. Gadsden, J. Yawney, Financial fraud: A review of anomaly detection techniques and recent advances, *Expert Syst. Appl.* 193 (C) (may 2022).
URL <https://doi.org/10.1016/j.eswa.2021.116429>
- [26] A. Sgueglia, A. Di Sorbo, C. A. Visaggio, G. Canfora, A systematic literature review of iot time series anomaly detection solutions, *Future Generation Computer Systems* 134 (2022) 170–186.
URL <https://www.sciencedirect.com/science/article/pii/S0167739X22001285>

- [27] F. Jiang, J. Yuan, S. A. Tsafaris, A. K. Katsaggelos, Anomalous video event detection using spatiotemporal context, *Comput. Vis. Image Underst.* (2011) 323–333.
URL <https://doi.org/10.1016/j.cviu.2010.10.008>
- [28] S. Calderara, U. Heinemann, A. Prati, R. Cucchiara, N. Tishby, Detecting anomalies in people’s trajectories using spectral graph analysis, *Comput. Vis. Image Underst.* (2011).
- [29] C. Li, Z. Han, Q. Ye, J. Jiao, Visual abnormal behavior detection based on trajectory sparse reconstruction analysis, *Neurocomputing* (2013) 94–100doi:10.1016/j.neucom.2012.03.040.
- [30] D. Gong, L. Liu, V. Le, B. Saha, M. R. Mansour, S. Venkatesh, A. Van Den Hengel, Memorizing normality to detect anomaly: Memory-augmented deep autoencoder for unsupervised anomaly detection, in: *2019 IEEE/CVF International Conference on Computer Vision (ICCV)*, 2019, pp. 1705–1714. doi:10.1109/ICCV.2019.00179.
- [31] D. M. Tax, R. P. Duin, Support vector data description, *Machine learning* (2004).
- [32] B. Schölkopf, J. C. Platt, J. Shawe-Taylor, A. J. Smola, R. C. Williamson, Estimating the support of a high-dimensional distribution, *Neural computation* (2001).
- [33] Z. Wang, Z. Chen, J. Ni, H. Liu, H. Chen, J. Tang, Multi-scale one-class recurrent neural networks for discrete event sequence anomaly detection, in: *Proceedings of the 27th ACM SIGKDD Conference on Knowledge Discovery & Data Mining*, 2021, pp. 3726–3734.
- [34] M. Sabokrou, M. Fayyaz, M. Fathy, R. Klette, Deep-cascade: Cascading 3d deep neural networks for fast anomaly detection and localization in crowded scenes, *IEEE Transactions on Image Processing* 26 (2017) 1992–2004.

- [35] T. N. Kipf, M. Welling, Semi-Supervised Classification with Graph Convolutional Networks, in: Proceedings of the 5th International Conference on Learning Representations, ICLR '17, 2017.
- [36] C. Zhong, L. Hu, Z. Zhang, Y. Ye, S. Xia, Spatio-temporal gating-adjacency gcn for human motion prediction, in: Proceedings of the IEEE/CVF Conference on Computer Vision and Pattern Recognition (CVPR), 2022, pp. 6447–6456.
- [37] Y.-F. Song, Z. Zhang, C. Shan, L. Wang, Constructing stronger and faster baselines for skeleton-based action recognition, *IEEE Transactions on Pattern Analysis and Machine Intelligence* (2022) 1–1doi:10.1109/TPAMI.2022.3157033.
- [38] S. Ioffe, C. Szegedy, Batch normalization: Accelerating deep network training by reducing internal covariate shift, in: F. Bach, D. Blei (Eds.), Proceedings of the 32nd International Conference on Machine Learning, Vol. 37, 2015, pp. 448–456.
- [39] M. Sabokrou, M. Fathy, M. Hoseini, Video anomaly detection and localisation based on the sparsity and reconstruction error of auto-encoder, *Electronics Letters* 52 (2016) 1122–1124.
- [40] W. Luo, W. Liu, D. Lian, S. Gao, Future frame prediction network for video anomaly detection, *IEEE Transactions on Pattern Analysis and Machine Intelligence* 44 (11) (2022) 7505–7520. doi:10.1109/TPAMI.2021.3129349.
- [41] M.-I. Georgescu, A. Bărbălău, R. T. Ionescu, F. Shahbaz Khan, M. Popescu, M. Shah, Anomaly detection in video via self-supervised and multi-task learning, in: 2021 IEEE/CVF Conference on Computer Vision and Pattern Recognition (CVPR), 2021, pp. 12737–12747.
- [42] T. R. Davidson, L. Falorsi, N. De Cao, T. Kipf, J. M. Tomczak, Hyperspher-

ical variational auto-encoders, 34th Conference on Uncertainty in Artificial Intelligence (UAI-18) (2018).

- [43] N. De Cao, W. Aziz, The power spherical distribution, Proceedings of the 37th International Conference on Machine Learning, INNF+ (2020).
- [44] M. I. Georgescu, R. Ionescu, F. S. Khan, M. Popescu, M. Shah, A background-agnostic framework with adversarial training for abnormal event detection in video, IEEE Transactions on Pattern Analysis and Machine Intelligence (2021). doi:10.1109/TPAMI.2021.3074805.
- [45] G. Bertasius, H. Wang, L. Torresani, Is space-time attention all you need for video understanding?, in: Proceedings of the International Conference on Machine Learning (ICML), 2021, p. 4.
- [46] D. P. Kingma, J. Ba, Adam: A method for stochastic optimization, CoRR abs/1412.6980 (2015).
- [47] S. Hochreiter, J. Schmidhuber, Long short-term memory, Neural Computation 9 (8) (1997) 1735–1780. doi:10.1162/neco.1997.9.8.1735.

Alessandro Flaborea. is a Ph.D. student at the Sapienza University of Rome. He received his degree in Computer Science from the University of Udine, Italy, and his master’s degree in Data Science from the Sapienza University of Rome. His research interests include few-shot learning, time series, video anomaly detection, and pose estimation.

Guido Maria D’Amely di Melendugno. is a Ph.D. student in Computer Science at the Sapienza University of Rome. After the master’s degree in Mathematics obtained at the Sapienza University of Rome, he focused on Computer Vision. His research interests lie in Text-Image Retrieval, Multimodal CV, Pose Forecasting, and Video Anomaly Detection.

Stefano D'Arrigo. is a Ph.D. student in Artificial Intelligence at the Sapienza University of Rome. He received a BSc in Computer Science at the University of Catania, Italy, and a MSc in Data Science at the Sapienza University of Rome. His research interests include pose estimation, video anomaly detection, and geometric deep learning.

Marco Aurelio Sterpa. is an MSc student at the Sapienza University of Rome. He received his bachelor's degree in Computer Science from the Sapienza University of Rome and is currently a second-year master's degree student in Data Science. His research interests include time series and video anomaly detection.

Alessio Sampieri. is a Ph.D. student in Data Science at the Sapienza University of Rome. He received his degree in Statistics for Management and master's degree in Data Science from the Sapienza University of Rome. His research interests include human motion and its forecasting, video analysis and understanding and geometric deep learning.

Fabio Galasso. heads the Perception and Intelligence Lab (PINLab) at the Dept. of Computer Science, Sapienza University of Rome (Italy).

His research interests include distributed and multi-agent intelligent systems, perception (detection, recognition, re-identification, forecasting) and general intelligence (reasoning, meta-learning, domain adaptation), within sustainable (low-power-consumption and constrained-computational-resource sensors and devices) and interpretable frameworks.